Mechanical basis for low-angle normal faulting in the Basin and Range province

H. J. Melosh

Lunar and Planetary Laboratory and Department of Geosciences, University of Arizona, Tucson, Arizona 85721, USA

Low-angle normal faults seem to violate the criterion that relates fault dip to stress orientation. To explain such faults one must postulate a 45° rotation of principal stress directions at mid-crustal depths, which is difficult to understand on the basis of previous elastic crust models. Such a stress rotation is shown to be a natural consequence of a low-viscosity lower crust.

DETAILED geological mapping in the Basin and Range of the western United States has recently revealed a type of fault that, at first sight, defies a simple mechanical explanation. Low-angle normal faults or detachments of large areal extent have been recognized in many areas of the Basin and Range province[1-3]. The large extent and extremely shallow dip of these low-angle normal faults, or detachment surfaces, indicates that the faults originally formed at low angles[4]. Where exposed, the footwall is generally foliated to mylonitic[5-7], indicating ductile strain at mid-crustal depths. Although the hanging wall presently exhibits a more brittle deformational style, low-angle slip probably began at mid-crustal depths near the brittle–ductile transition.

The problem with low-angle normal faults is that observations on rock fracture indicate that most faults form as shear fractures at orientations of ±30° to the maximum compressional stress axis. Anderson[8] argued that, near the Earth's surface, one principal stress direction must be perpendicular to the surface because shear stresses vanish at a free surface. Depending on whether this perpendicular principal stress is the maximum, minimum or intermediate stress, the resulting faults are either normal, thrust or strike-slip with dips of 60°, 30° or 90° (vertical) respectively. The only way low-angle normal faults can form as shear fractures is if the principal stress directions rotate rapidly between the surface and depths ranging from 6 to 10 km where low-angle normal faults are believed to form. The alternative, that low-angle normal faults represent a new type of fracture in which the slip plane is nearly perpendicular to the maximum compressive principal stress, is not supported by any experimental evidence on rock fracture of which I am aware. But it seems equally difficult to understand how, in a broad terrane of relatively uniform crustal thickness, principal stress directions can rotate by 30° or 45° between the surface and mid-crustal depths. Where do the large shear stresses necessary to cause the rotation come from? Recent models that treat the crust as an elastic plate[9,10] have shown that large principal-axis rotations are possible in the vicinity of large compressive, flexural or shear loads where shear stresses change rapidly, but such explanations imply special circumstances that involve hidden sub-crustal forces or structures.

A more general explanation of stress rotation in the Basin and Range can be derived from the rheological structure of the crust in this high heat-flow region. Figure 1*a* shows the effective viscosity η_{eff} as a function of depth in a crust and upper mantle extending at a mean strain rate of 2×10^{-15} s^{-1} (assuming 100% Basin and Range extension over 15 Myr; C. Chase, personal communication) in a model crust similar to that of ref. 11. A 10-km-thick upper crust is rheologically identical to westerly granite, a 10-km-thick lower crust acts like Maryland diabase, and the upper mantle is dominated by olivine. Although some aspects of this model may be unrealistic (the effect of varying water content is not addressed here, and the transition from upper crust to lower crust is probably gradual, thus reducing the viscosity peak at the top of the lower crust), the general pattern is believed to be accurate. The mechanical implication of this structure is shown in Fig. 1*b*, where the Maxwell time, $\tau = \eta_{eff}/\mu$, is plotted as a function of depth (μ is shear modulus). The crust responds elastically to loads applied for time intervals shorter than the Maxwell time, but behaves as a viscous fluid for loads applied for longer periods. In the Basin and Range, only the upper few kilometres of the crust behave elastically for loads that exist for more than ~1 Myr, and in the lower part of the crust the Maxwell time is only ~10,000 yr. These short times are due to both the relatively high heat flow of the Basin and Range, as rock viscosity is strongly temperature-dependent, and also to the relatively high extensional strain rate, as the effective viscosity also decreases with increasing strain rate (see, for example, ref. 12).

In the Basin and Range, the crust and upper mantle can be thought of as a thin upper layer, which behaves elastically, grading into a lower viscous layer, which has one or more additional elastic layers underneath. Such a crust can clearly

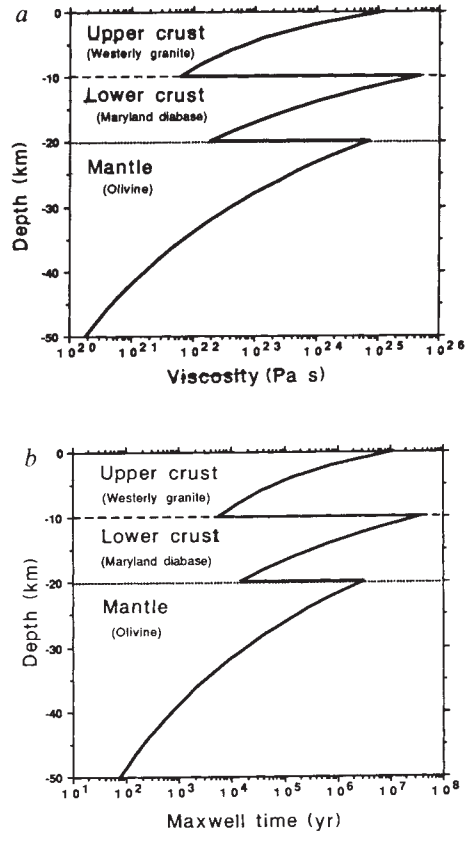

FIG. 1 Rheological structure inferred for the present Basin and Range using the thermal gradient of Smith and Bruhn[11] and the rheological data of Kirby and Kronenberg[12,17] for the materials indicated; *a*, shows the viscosity as a function of depth and *b*, shows the Maxwell time. Elastic moduli in the crust are from Dziewonski *et al.*[22].

not be treated as a uniform, homogeneous elastic slab. This structure is the key to understanding the principal-stress rotations apparent from low-angle normal faults. Here I show that if the upper elastic layer is displaced horizontally with respect to a lower elastic layer, the intervening viscous layer is subjected to simple shear. Such displacement is a natural result of localized faulting in the upper crust, opposed to uniform stretching in the lower elastic layer(s). The principal stress directions in the viscous layer thus become orientated at 45° to the vertical, consistent with the formation of low-angle ductile faults—by the Mohr–Coulomb failure law, brittle rocks with angles of internal friction near 30° fail along planes at angles of ±30° to the compressive stress axis, but in ductile failure the angle is expected to be ±45°. Experimental confirmation of this expectation is, however, sketchy (T. and J. Tullis, personal communication). The principal-stress rotation between the surface and mid-crustal depths is thus due to the change in rheology from elastic to viscous at these depths, coupled with some differential slip between the layers.

Analytical model of extension

It is easy to show that the principal stress directions in a viscoelastic layer sheared between two elastic layers approach an orientation of 45° to the vertical within a few Maxwell times of the application of the shear. The initial stress state of any part of the crust is generally complicated because it depends on the history as well as the present geological circumstances of that particular piece of crust. However, in general, within the constraints of keeping the analysis simple, suppose that in some region the vertical stress is $\sigma_{zz} = \rho g z$, where z is depth, g the acceleration due to gravity, and, for simplicity, we assume that the density ρ of the crust is uniform. Let the initial horizontal stress be $\sigma_{xx} = k\sigma_{zz}$, where k is a constant in accordance with observation[13], and the shear strain rate $\dot{\varepsilon}_{xz} = \dot{\varepsilon}_0$ is constant. Solution of the Maxwell viscoelastic constitutive relations in conjunction with the stress equilibrium equations shows that the time evolution of the stresses is

$$\sigma_{xx}(t) = \sigma_{zz} + (k-1)\sigma_{zz}\mathrm{e}^{-t/\tau} \tag{1a}$$

$$\sigma_{zz}(t) = \rho g z \tag{1b}$$

$$\sigma_{xz}(t) = \sigma_{xz}(0)\mathrm{e}^{-t/\tau} + 2\eta\dot{\varepsilon}_0(1-\mathrm{e}^{-t/\tau}) \tag{1c}$$

where τ is the Maxwell time, $\tau = \eta/\mu$, η is viscosity and μ is the elastic shear modulus.

Within a few Maxwell times, these stresses approach a steady state in which $\sigma_{xx} = \sigma_{zz} = \rho g z$, $\sigma_{xz} = 2\eta\dot{\varepsilon}_0$. The angle θ between the vertical and the maximum compressive principal stress is (equation 2-34 in ref. 14)

$$\tan 2\theta = \frac{2\sigma_{xz}}{\sigma_{xx} - \sigma_{zz}} \tag{2}$$

as σ_{xx} approaches σ_{zz} the right-hand side of this equation approaches infinity and θ therefore approaches 45°, as described (see Fig. 2). A somewhat similar idea was proposed by Bradshaw and Zoback[15], who investigated the refraction of principal stress directions between layers of differing viscosity, although they did not discuss viscoelastic stress relaxation or make it clear that differential slip across the layers is necessary. The above result corresponds to theirs in the limit of infinite viscosity contrast (that is, elastic layer against viscous layer).

Simple shear of a viscoelastic layer thus results in a pure shear stress state within a few Maxwell times. The memory of any initially different stress state is completely lost as viscous relaxation proceeds. The final state of stress at depth is thus consistent with low-angle ductile shear faults, whose failure planes are located at ±45° to the principal stress directions, according to the Mohr–Coulomb construction. The problem of explaining the occurrence of low-angle normal faults in the Basin and Range thus reduces to one of determining how the uppermost elastic layer can slip relative to one of the deeper-lying elastic layers, as the above analysis shows that when such slip occurs the principal stress axes are always rotated in the intervening viscoelastic layer.

Consider the simple model of Basin and Range extension shown in Fig. 3. An elastic crustal block of length L and thickness h_{eff} is underlain by a viscous lower crust of thickness h_{lc}. Beneath this lower crust lies stiffer upper mantle which is under sufficient pressure that it flows in a ductile (not viscous) fashion when stresses within it exceed its yield strength, extending at a uniform strain rate $\dot{\varepsilon}$. The coordinate system is chosen such that the velocity of the upper mantle relative to the upper crust is $v_{\mathrm{b}} = \dot{\varepsilon}x$, so that the centre of the crustal block is stationary with respect to the upper mantle, but the differential velocity increases linearly with increasing distance from the block's centre. This is the situation expected for an extending mantle beneath a brittle crust that cannot support large strains without fracture. The fractures are represented by vertical breaks at $x = \pm L/2$ in this simple model. The stress acting across these breaks is set equal to a constant, $\sigma_{xx}^{\mathrm{fit}}$, which is less than the breaking strength of the crust. The extensional strain rate in the brittle crustal block is essentially zero: the regional strain imposed by the extending upper mantle is accommodated by relative motion of crustal blocks at their edges, where the relative velocity is $\Delta v = \dot{\varepsilon}L$.

The viscous lower crust in this model, $-h_{\mathrm{lc}} < z < 0$ is thus

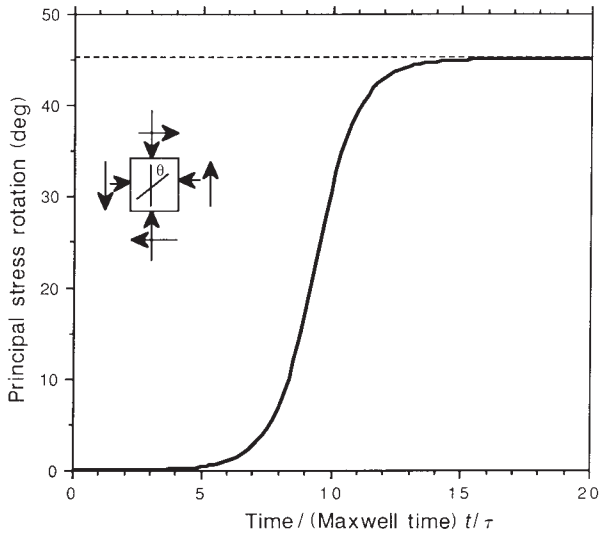

FIG. 2 Rotation of principal stress axes in a viscoelastic material as a function of time, derived from equations (1) and (2). After a period of ~10 Maxwell times the principal stresses rotate to an angle of 45°. The inset shows the definition of rotation angle θ and the short arrows illustrate the applied stresses.

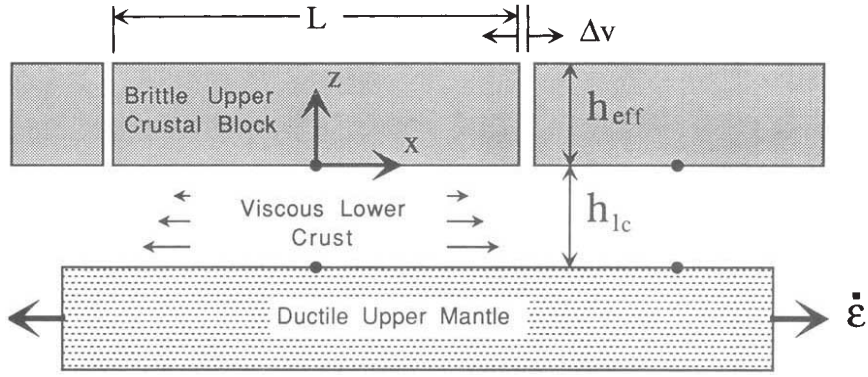

FIG. 3 Schematic illustration of the analytical crustal-block model for Basin and Range extension. An effectively rigid upper-crustal block is separated from a ductile extending upper mantle by a viscous lower crust.

subject to a differential velocity between its top, which is in contact with the brittle non-extending crust and its bottom, which is in contact with the uniformly extending mantle. The components of the velocity field in the lower crust are determined by the boundary conditions and the assumption that the horizontal velocity gradient is linear (good for a thin lower crust):

$$v_x(x, z) = -\dot{\varepsilon}\frac{xz}{h_{lc}} \tag{3a}$$

$$v_z(x, z) = \dot{\varepsilon}\frac{z^2 - h_{lc}^2}{2h_{lc}} \tag{3b}$$

where v_z is determined from v_x and the condition of incompressibility, $\nabla \cdot \mathbf{v} = \mathbf{0}$. As $h_{lc} \ll L$, in general $v_z \ll v_x$: the z-component of velocity corresponds to a uniform thinning due to extension that is much slower than the horizontal stretching. The viscous (non-lithostatic) stresses developed in the lower crust may be calculated from the velocity field by the usual constitutive relations $(-h_{lc} < z < 0)$,

$$\sigma_{xx}^{lc} = 2\eta\frac{\partial v_x}{\partial x} = -2\eta\dot{\varepsilon}\frac{z}{h_{lc}} \tag{4a}$$

$$\sigma_{zz}^{lc} = 2\eta\frac{\partial v_z}{\partial z} = 2\eta\dot{\varepsilon}\frac{z}{h_{lc}} \tag{4b}$$

$$\sigma_{xz}^{lc} = \eta\left(\frac{\partial v_x}{\partial z} - \frac{\partial v_z}{\partial x}\right) = -\eta\dot{\varepsilon}\frac{x}{h_{lc}} \tag{4c}$$

Note that all the stresses are scaled by the same factor of viscosity multiplied by the strain rate, $\eta\dot{\varepsilon}$, so that the principal-stress rotation angle, being a ratio (equation (2)), is independent of either viscosity or strain rate. At the top of the lower crust, $z = 0$, σ_{xz}^{lc} is the only non-zero stress, and the principal stress axes are rotated to 45° here. Furthermore, throughout most of the lower crust $z \ll x$, so the principal stress axes are rotated close to 45° everywhere except near the centre at $x = 0$.

The shear thus developed in the lower crust exerts a basal shear stress σ_b on the brittle upper crust, where $\sigma_b = 2\eta\dot{\varepsilon}_{xz} = \eta\dot{\varepsilon}(x/h_{lc})$. By the stress equilibrium equations, this basal shear results in an extensional stress in the overlying brittle lithosphere[16] because the shear stress must decrease linearly to zero at the free surface at the top of the upper crust. The non-lithostatic stresses in the brittle upper crust are thus $(0 < z < h_{eff})$

$$\sigma_{xx}^{uc} = \frac{\eta\dot{\varepsilon}}{2h_{eff}h_{lc}}\left[\left(\frac{L}{2}\right)^2 - x^2\right] + \sigma_{xx}^{fit} \tag{5a}$$

$$\sigma_{zz}^{uc} = 0 \tag{5b}$$

$$\sigma_{xz}^{uc} = \frac{\eta\dot{\varepsilon}}{h_{lc}}\left(1 - \frac{z}{h_{eff}}\right)x \tag{5c}$$

where σ_{xx}^{fit} is the stress at the ends of the crustal block. The horizontal stress is smallest at the ends of the crustal block and maximum in the middle. If this stress were to cause the crustal block to break up further, the site of the next fracture would thus be in its middle. The shear stress in the crust declines from σ_b at the bottom to zero at the top, as it must. The vertical stress is zero (the lithostatic stress must be added to the above stresses to get the full stress field, but because the lithostatic stress plays no part in controlling principal stress direction it can be safely neglected here). Equations (5a–c) show that throughout most of the upper crust $\sigma_{xx}^{uc} \gg \sigma_{xz}^{uc}$, because $L \gg h_{eff}$, so that principal-axis rotations are small, and normal faults would be expected to form in the usual 60° dip orientation in this region.

The principal stress directions for this model are shown in Fig. 4. The length of the unfractured crustal block is 200 km and the thickness of the upper and lower crust are 6 km and 14 km, respectively. No other parameters, such as viscosity or strain rate, enter into the determination of the stress directions. It is clear that in the vicinity of the ends of the crustal blocks the orientations of the bounding faults should undergo a sharp change as they cross the upper/lower crust boundary, changing abruptly from the usual 60° dip in the upper crust to nearly flat in the lower crust (assuming that faults in the ductile zone form at ±45° to the compressional axis, as predicted by Mohr–Coulomb theory). Of course, the upper/lower crustal boundary is actually gradational, being established by the decrease in

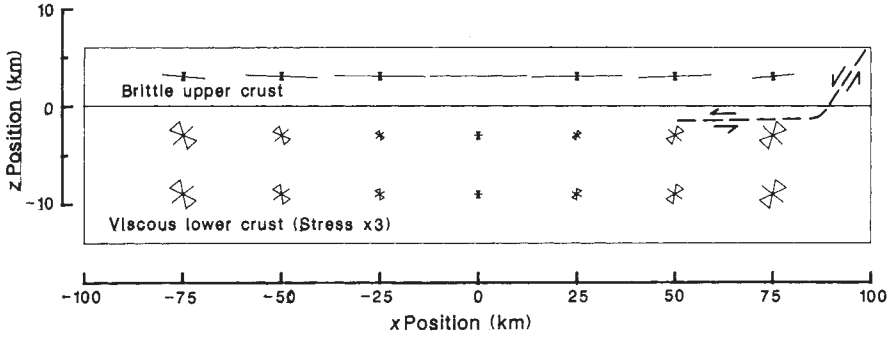

FIG. 4 Stresses in the analytical crustal-block model derived from equations (5a–b). The triangular symbols represent compressional principal stresses, the lines are extensional principal stresses, and the symbol size is proportional to the size of the stress. Note the exaggeration of the symbol size in the lower crust. The dashed line illustrates the geometry of a fault expected to form under the influence of this stress field.

Maxwell time with depth, so the orientation of the fault planes should rotate from steep to nearly flat over some depth interval, but the rate at which the Maxwell time declines with depth (Fig. 1*b*) is so high that this interval will be at most a kilometre or two.

Finite-element model of extension

Although the above analytical model displays most of the behaviour necessary to illustrate stress rotation in the lower crust, it may be argued that the vertical boundaries of the edges of the crustal blocks are unrealistic, that the measured rheology of crustal rocks is non-newtonian, and that the boundary between upper and lower crust is artificially chosen to lie at a fixed depth. To answer this criticism, I also present the results of a finite-element computation designed to be as realistic a representation of the Basin and Range crust and upper mantle as possible.

The basic structure of this plane-strain finite-element model of the Basin and Range extension is that of an upper and lower crust that together are 20 km thick. The rheological model is similar to that illustrated in Fig. 1, except that the transition between the upper and lower crust is more gradational to avoid the complication of the mid-crustal lithosphere in Fig. 1. The flow laws used are from refs 12 and 17. The crust is underlain by a stiff upper mantle that stretches homogeneously throughout the computation. The stiffness of this layer allows it to be modelled as a relatively thin 5 km-thick layer that is allowed to slip freely in the x-direction, but which is constrained to zero vertical deformation at its base. Experiments with grids as deep as 175 km show no differences between the shallow and deep grids, whereas the shallow grid allows much more resolution in the horizontal direction. Freely slipping faults are introduced at 50-km intervals in the upper crust using the recently developed 'slippery-node' method[18]. Note that the stress axes in the vicinity of the fault in Fig. 5 are rotated so that one principal stress is perpendicular to the fault plane, as required by the slip condition. The model is extended at a strain rate of $2\times10^{-15}\,s^{-1}$, and the stresses that develop near the fault after 26,000 years are plotted in Fig. 5. Only deviatoric stresses are plotted here. Such a plot avoids problems with a mild instability in the finite-element code known as 'pressure checkerboarding' (ref. 19) that develops under the application of large viscous strains. Although this instability limits the accuracy with which the pressure field can be determined, it does not affect the accuracy of either the deviatoric stresses or the displacements[19]. The finite-element grid is much broader than the region shown, minimizing the effect of artificial (velocity) boundary conditions at its ends: the entire grid is 400 km long and 25 km deep and contains 8 faults, 920 elements and 1,032 nodes. The section shown in Fig. 5 focuses on the end of one crustal block.

It is clear from Fig. 5 that stresses are rotated at mid-crustal levels. The greatest (~45°) rotation occurs at ~6 km depth beneath the hanging wall of the steep segment of the fault, although smaller rotations are apparent even at depths of 4 km. The lower viscosities at depths of 7 km and deeper prevent the development of any significant deviatoric stresses at the time of this plot, although at earlier times 45° stress rotations occurred at deeper levels. Any faults that follow the directions dictated by these stress directions will thus make a sharp turn at the brittle-ductile transition, flattening out in a manner consistent with that inferred for the low-angle normal faults in the Basin and Range province.

Stress and slip on the boundary faults

It may seem surprising that the horizontal stress near the fault in Fig. 5 does not fall to zero. Although the fault surface itself enforces a condition of zero resolved shear stress, and although it cuts completely through the elastic part of the upper crust, a significant horizontal stress σ_{xx}^{fit} nevertheless develops at the fault. The ultimate origin of this stress is in the viscous lower crust. Although the fault slips freely, the geometry of the fault requires that a given horizontal slip must be accompanied by a corresponding vertical slip, as open gaps cannot develop in the Earth. But the upper-crustal block rests on a viscous substratum that must flow from beneath the hanging wall to the footwall to accommodate the vertical displacement (see Fig. 6). This flow requires a stress to drive it, and this stress ultimately appears as an additional horizontal stress σ_{xx}^{fit} which acts in the vicinity of the end of the upper-crustal block. (Note that the development of great topographic differences across the fault may also contribute to this stress. Such stresses are ignored here as being generally smaller than the viscous contribution and entirely negligible if erosion and deposition outpace tectonic uplift.)

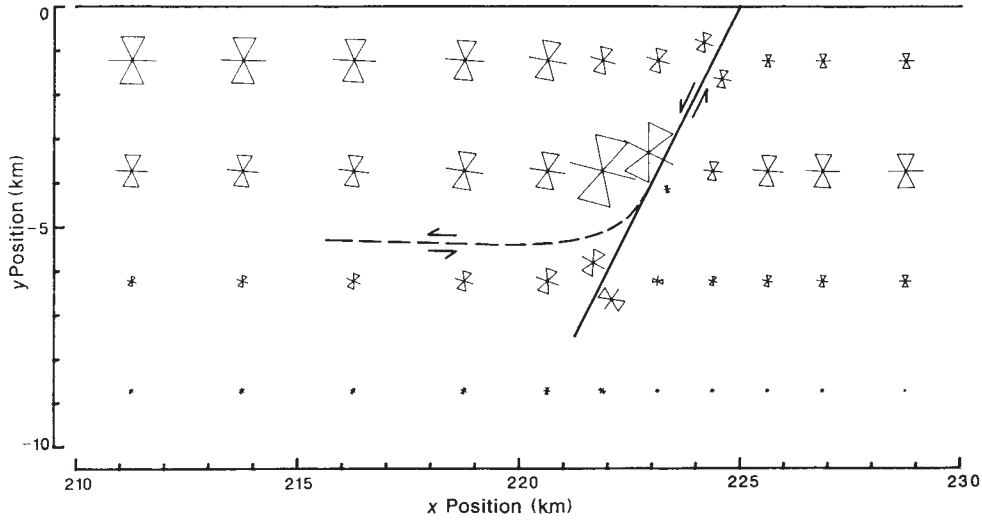

FIG. 5 Deviatoric stresses in a finite-element model of crustal extension 26,000 years after the beginning of extension at a strain rate of $2\times10^{-15}\,s^{-1}$. The viscoelastic material obeys a power-law flow relation with $n=3$ and has the following effective viscosities (at the above strain rate): $\eta_{eff}=3\times10^{24}$ Pa s between 0 and 2.5 km depth, 4×10^{22} Pa s from 2.5 to 5 km, 4×10^{21} Pa s from 5 to 7.5 km, 1×10^{22} Pa s from 7.5 to 10 km, 6×10^{20} Pa s from 10 to 20 km, then 10^{24} Pa s from 20 to 25 km (stiff upper mantle, for which $n=3.5$). The largest symbol represents a stress of 7.35×10^{7} Pa. The horizontal dashed line illustrates the trend of a fault forming under the influence of the stress field in the lower crust at this time.

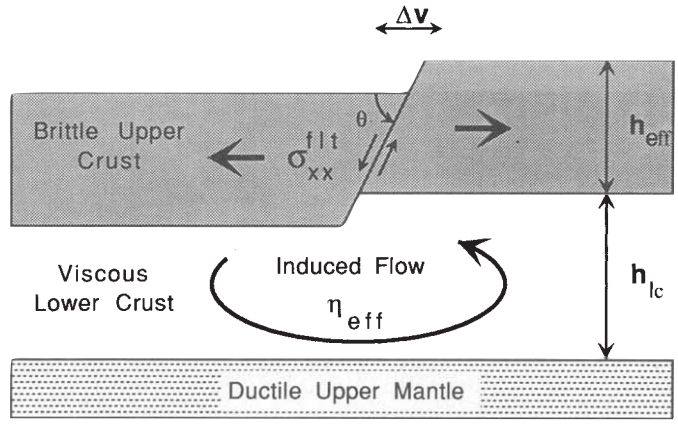

FIG. 6 Schematic illustration of flow in the vicinity of a fault cutting an upper-crustal block and the induced flow that results in a horizontal stress σ_{xx}^{fit} associated with slip on the fault.

A simple geometrical derivation gives the following approximate equation

$$\sigma_{xx}^{fit} \approx \left(\frac{2\eta_{eff}}{h_{eff}}\right)\Delta v \qquad (6)$$

In this equation it is remarkable that there is no dependence on either fault dip or on the thickness of the lower crustal layer, a conclusion that is supported by a number of finite-element runs with different fault dips and crustal thickness. It was also verified that equation (6) roughly holds when the crustal block is terminated by a graben rather than by a single normal fault: for a graben σ_{xx}^{fit} is lowered by less than a factor of two.

The existence of the stress σ_{xx}^{fit} at the ends of the otherwise free upper-crustal blocks may play a primary part in determining whether extension takes place by the creation and separation of large crustal blocks, as in the Basin and Range, or whether it is accommodated on many closely spaced normal faults. If σ_{xx}^{fit} is small when compared to the strength of the crust then large relatively rigid blocks can be expected to develop in the extended region, but if σ_{xx}^{fit} is much larger than the crust's strength then it would be expected to break up into many small fragments. In the finite-element simulation of Fig. 5, σ_{xx}^{fit} was $\sim 7\times10^{7}$ Pa, corresponding to a viscosity η_{eff} of 6×10^{21} Pa s. This relatively large stress may preclude the formation of isolated crustal blocks, which would thus require a lower viscosity. Such a lower viscosity may have been realized by a higher thermal gradient in the Basin and Range at the time of the major detachment faulting than is observed today.

Conclusions

The above results from both analytical and finite-element models illustrate the principal conclusion that it is the rheological change between the upper and lower crust that is responsible for the low-angle normal faults observed in the Basin and Range province, not a special or local loading condition. The astute reader will note that the largest stress differences are in the brittle upper crust, not in the viscous lower crust. To explain the occurrence of low-angle normal faults, we must suppose that the earthquake that accompanies sudden slip on the fault initiates near the base of the brittle crust. Displacement during the event propagates rapidly towards the surface along a steep fault as seen in the 1983 Borah Peak earthquake[20]. Further down in the viscoelastic lower crust strain propagation may be slower and the direction taken by the propagating rupture is either guided into a horizontal orientation by the ambient stress field after the seismic event or, more likely, may accumulate by aseismic slip for a long time before the event. This may explain the oft-cited observation that, whereas low-angle normal faults seem to be common in the Basin and Range, low-angle earthquake focal mechanisms are not.

The fact that a change in rheology can induce drastic changes in fault orientation is not confined to the Basin and Range problem alone. On a much smaller scale, it is frequently observed that when faults in competent bedded rocks cross horizons of more deformable material, such as shale horizons or evaporite beds, the cross-cutting faults suddenly change direction, being 'refracted' across the deformable bed. This refraction may be seen as simply the result of viscoelastic stress relaxation in the deformable bed, coupled with a small amount of shear displacement between the surrounding competent units. A theory of fault refraction along these lines has already been presented by Bradshaw and Zoback[15].

Similarly, thrust faults are often inferred to 'root' in a horizon of especially deformable rock in which their orientations become parallel to the bedding[21]. This situation is sometimes called 'decollement' faulting in compressional environments or 'detachment' faulting when extension dominates. This situation may again be simply an example of the 45° rotation of stresses that invariably occurs in a sheared viscoelastic layer. Stress (and hence fault) rotation due to a rheologically weak layer is thus a common situation in geology, and the low-angle normal faults observed in the Basin and Range province and in metamorphic core complexes should only be regarded as unusually large examples of this phenomenon. □

Received 4 September; accepted 6 December 1989.

1. Proffett, J. M. J. *Geol. Soc. Am. Bull.* **88,** 247–266 (1977).
2. Crittenden, M. D. J., Coney, P. J. & Davis, G. H. *Mem. geol. Soc. Am.* **153** (1980).
3. Frost, E. G. & Martin, D. L. *Mesozoic–Cenozoic Tectonic Evolution of the Colorado River Region, California, Arizona and Nevada* (Cordilleran, San Diego, 1982).
4. Davis, G. A., Anderson, J. L., Frost, E. G. & Shackelford, T. J. *Mem. geol. Soc. Am.* **153,** 79–129 (1980).
5. Wernicke, B. *Nature* **291,** 645–648 (1981).
6. Lee, J., Miller, E. L. & Sutter, J. F. *Spec. Publ. geol. Soc. Am.* **28,** 267–298 (1987).
7. Davis G. A., Lister, G. S. & Reynolds, S. J. *Geology* **14,** (1986).
8. Anderson, E. M. *The Dynamics of Faulting* 1–206 (Oliver and Boyd, Edinburgh, 1951).
9. Yin, A. *Tectonics* **8,** 469–482 (1989).
10. Spencer, J. E. & Chase, C. G. *J. geophys. Res.* **94,** 1765–1775 (1989).
11. Smith, R. B. & Bruhn, R. L. *J. geophys. Res.* **89,** 5733–5762 (1984).
12. Kirby, S. H. & Kronenberg, A. K. *Rev. Geophys.* **25,** 1219–1244 (1987).
13. McGarr, A. & Gay, N. C. *A. Rev. Earth planet. Sci.* **6,** 405–436 (1978).
14. Turcotte, D. L. & Schubert, G. *Geodynamics: Applications of Continuum Physics to Geological Problems* 1–450 (Wiley, New York, 1982).
15. Bradshaw, G. A. & Zoback, M. D. *Geology* **16,** 271–274 (1988).
16. Melosh, H. J. *Pure appl. Geophys.* **115,** 429–439 (1977).
17. Kirby, S. H. & Kronenberg, A. K. *Rev. Geophys.* **25,** 1680–1681 (1987).
18. Melosh, H. J. & Williams, C. A. *J. geophys. Res.* **94,** 13961–13973 (1989).
19. Hughes, T. J. R. *The Finite Element Method* Ch. 4 (Prentice-Hall, Englewood Cliffs, NJ, 1987).
20. Stein, R. S. & Barrientos, S. E. *J. geophys. Res.* **90,** 11,355–11,366 (1985).
21. Suppe, J. *Principles of Structural Geology* 1–537 (Prentice-Hall, Englewood Cliffs, NJ, 1985).
22. Dziewonski, A. M., Hales, A. L. & Lapwood, E. R. *Phys. Earth planet. Inter.* **10,** 12–48 (1975)

ACKNOWLEDGEMENTS. Greg Radel participated in the early finite-element work on this problem, and I thank Clem Chase and Terry and Jan Tullis for discussions on this approach to low-angle normal faults.